Influence of eruptive style on volcanic gas emission chemistry and temperature

Clive Oppenheimer[1*], Bruno Scaillet[2], Andrew Woods[3], A. Jeff Sutton[4], Tamar Elias[4], Yves Moussallam[1,5]

1. Department of Geography, University of Cambridge, Cambridge, CB2 3EN, UK.
2. Institut des Sciences de la Terre d'Orléans, CNRS/Université d'Orléans/BRGM, 1a Rue de la Férolerie 45071, Orléans, France
3. BP Institute, University of Cambridge, Madingley Road, Cambridge CB3 0EZ, UK
4. Hawaiian Volcano Observatory—U.S. Geological Survey, PO Box 51, Hawai'i National Park, HI, 96718, USA.
5. Laboratoire Magmas et Volcans, Univ. Blaise Pascale – CNRS – IRD, OPGC, 63000 Clermont-Ferrand, France

As magmas ascend in the crust, they exsolve volatiles (e.g., carbon, oxygen, sulphur, hydrogen and chlorine). Gas bubbles evolve chemically and physically as magma decompression and crystallization proceed. In less viscous magmas, bubbles may rise at faster rates than the melt. While it is generally assumed that gas remains in thermal equilibrium with the melt, the relationship between gas and melt redox state in degassing magmas is debated. Here we report equilibrium conditions for gas emissions from the summit lava lake of Kīlauea volcano, Hawaii, calculated from gas abundances measured in the atmosphere by absorption spectroscopy. Our observations, which span a transition between more and less vigorous degassing regimes, reveal a remarkable temperature span

of up to 250°C. They also show a progressive increase of the redox state of the gas, relative to solid rock buffers, with decreasing gas temperature. We explain both phenomena as the result of variation in gas bubble size, and show that even for magmas more viscous than those encountered at Kīlauea, fast-rising bubbles can cool adiabatically and lose the redox signature of their associated melts. Our findings reveal a hitherto unrecognized process that can result in rapid changes in abundances of redox-sensitive gas species. Gas composition is monitored operationally at many volcanoes in support of hazard assessment but, often, consecutive sets of observations are time averaged. This can mask variability arising from the dynamics of degassing. Further, such redox decoupling between gas and melt as we observe calls for caution in using lava chemistry to infer the composition of associated volcanic gases.

The redox state of magmatic gases is pertinent to understanding atmospheric evolution[1] and ore formation[2], and bears on interpretation of gas geochemical data for volcanic hazard evaluation[3]. Gas ratios such as CO_2/CO, SO_2/H_2S and H_2O/H_2 are redox sensitive and may show complex variations associated with changes in eruptive style[4,5]. Numerical models show that, during magma ascent, melt-gas equilibria can drive magmatic redox state away from that of the reservoir or source region[6,7]. Such models assume, however, maintenance of thermal and chemical equilibrium between fluid and melt during decompression. While this assumption may hold for more viscous magmas, it may not be valid for basalts, by far the dominant product of global volcanism. For such low viscosity melts, physical models predict that decoupling between gas and melt is likely during ascent[8]. Here we consider the case for the ongoing basaltic eruption at Kīlauea volcano, Hawaii.

Composition of Kīlauea gas emissions

The bulk of gas geochemical data for Kīlauea stem from laboratory analyses of samples collected in the field, with necessary corrections made to account for air contamination, back-reaction during cooling, and interaction with sampling apparatus or host rocks[9,10]. More recent surveys have used open-path Fourier transform infrared spectroscopy (OP-FTS) to estimate relative proportions of C-, S- and halogen-bearing species[11], and the pressure of gas segregation and its relationship to eruption style[12]. We extend this approach by measuring the redox-sensitive species carbonyl sulfide (OCS), which permits evaluation of gas redox state with high-temporal resolution[13]. Previous work at Kīlauea, based on collection of gas samples, reached the conclusion that melt or rock buffers the gas redox state via oxygen exchange, even below the basalt solidus[9]. We revisit this hypothesis in the light of precise OP-FTS determinations of the molecular composition of gas emissions from the summit lava lake of Kīlauea volcano.

The spectrometer was positioned at the rim of Overlook Vent in Halema'uma'u crater and viewing towards the lava surface, which acted as the infrared source, approximately 200 m distant (Fig. 1a; Methods). Gases emitted from the lava lake surface, following ascent through the magma, continually crossed the spectrometer's field-of-view. Our observations spanned two degassing regimes: initially, the lake surface motion was sedate (Fig. 1b) with sporadic isolated bubble bursts, but we later captured an episode of vigorous degassing associated with sustained lava spattering at points along the lake perimeter, driven by the ascent and rupture of bubbles of up to several metres in diameter (Fig. 1c and S5). During this more energetic activity, we directed the spectrometer's field-of-view toward one of the spatter sources to maximize the contribution of its associated gas emission to the recorded absorption spectra. Over the long term, these degassing regimes are found to alternate, with spattering being the more prevalent[14].

We analyzed the abundances of H_2O, CO_2, CO, OCS, SO_2, HF and HCl in each spectrum acquired, correcting for water and CO_2 contributions from ambient air so as to yield relative gas contents for these seven species (Methods). Spectra were recorded approximately every 5 s, and we regard each as a temporally-discrete gas sample. The average composition, based on 995 spectra spanning the two degassing regimes, is as follows (all quantities in mol%): H_2O 91.6; CO_2 4.37; SO_2 2.89; CO 0.089; HCl 0.047; HF 0.030; OCS 0.00031. The mean molar ratios of SO_2/HCl and H_2O/CO_2 are ~68 and ~25, respectively. This composition is more water-rich and sulphur-poor than some prior measurements of summit degassing from Kīlauea[15], though comparable to others[16]. Certain molecular ratios, such as CO_2/CO vary significantly (Fig. S1) for reasons explored below. The CO_2/H_2O ratios for the two degassing regimes overlap.

Low-pressure degassing

The high water content suggests the magma has degassed its complement of volatiles up to atmospheric pressure[12] , consistent with interpretations of variability in lava lake level, gas chemistry and bulk outgassing[17]. To corroborate this, we re-examined analytical data for lavas dredged from the Puna ridge, which trends northeast of Kīlauea, reaching about 6 km below sea level[18,19]. These lavas were quenched as they erupted on the seabed, and span a wide range of depths (and hence ambient water pressures). The volatile contents in their glassy rinds enable calculation of equilibrium gas compositions and eruption pressures using solubility laws for equivalent melts[20,21,22,23] combined with gas equilibrium constants for the C-O-H-S system[24].

Although the recovered samples represent different eruptions, a conspicuous trend of increasing H_2O with decreasing pressure emerges (Fig. 2a). Taken with the near 1:1 correlation between calculated and collection pressures (Fig. 2b), it demonstrates that this lava suite faithfully

captures the first-order characteristics of degassing of shallow magmas beneath Kīlauea. Extrapolation of the Puna trend towards atmospheric pressure indicates that the gases we measured with OP-FTS must have maintained gas-melt equilibrium over much of their ascent path into the lava lake that feeds the plume. Gas-melt separation at significant depths would be recorded by gas compositions richer in CO_2 (i.e., a water mole fraction of 0.6 at about 30 bar near the base of the lava lake, Fig 2a), such as observed for some explosive events at Stromboli[5]. Sulfur and chlorine contents in the quenched glass of the Puna samples further substantiate this conclusion. The calculated trend, using a fluid-melt partition coefficient for Cl of 10 (refs. 25; 26), shows consistently increasing molar S/Cl ratio as pressure falls, reaching, at atmospheric pressure, ~60 (NNO = Nickel-Nickel Oxide, Fig. 2c), consistent with the value of ~68 that we observe in the gas emission.

Equilibrium temperature and redox calculations

Having established that the gas emissions from the lava lake have equilibrated to atmospheric pressure, we can use our measurements of CO, CO_2, SO_2 and OCS in the gas plume to determine, spectrum-by-spectrum, the fO_2 and equilibrium temperature of the emitted gas (Fig. 3; Methods). Two striking features emerge from the data distribution. First, the computed equilibrium temperatures span a wide range, from about 900 to 1150˚C, extending below the solidus of Kīlauea basalt (980˚C; ref. 27). The higher computed temperatures are mostly associated with the mild degassing regime and the lower temperatures with the spattering episode but there is overlap between the two. Second, the temperature range corresponds to a change in the computed fO_2 values from slightly above the Quartz-Fayalite-Magnetite (QFM) redox buffer at 1150˚C to slightly above the NNO redox buffer at 900˚C. We consider first the implications of the temperature variation and then those of the relative fO_2 shift.

Effects of variable bubble size

The wide range in calculated temperatures suggests gas cooling accompanying near adiabatic expansion of bubbles during ascent through the magma column. To test this hypothesis, we developed a simple thermodynamic model accounting for the radiative effects and expansion of bubbles due to decompression (Methods). This permits calculation of the degree of cooling of a rising bubble as a function of melt viscosity and final bubble size, which control speed of ascent (Fig. 4). The effect is strongest when the conductive heat flux from the melt is unable to keep pace with the work done as the bubble expands, i.e., in the case of larger bubbles rising in lower viscosity melts. For a typical viscosity of Kīlauea basalt of order 100 Pa s, a 2-m-radius bubble (as measured at the surface) has cooled ~95˚C, and a 3-m-radius bubble has cooled about 170˚C. Due to the accelerating ascent of bubbles as they expand and the decrease in gas emissivity at low pressure, the cooling is most pronounced in the final tens of metres of passage below the surface, i.e., within the lava lake.

This analysis leads us to view the computed equilibrium temperature for an individual spectrum (Fig. 3) as a proxy for bubble size population at an instant in time. As lake degassing becomes more vigorous, with larger bubbles reaching the surface and dominating the gas plume chemical signature that we record, gas temperatures drop due to increased cooling. Gas chemistry thus reflects the dynamics of degassing of the magma in the lake such that measurements made during even a brief period of variable activity yield a range of computed equilibrium temperatures. Each measurement captures the gas signature at an instant in time and cautions against temporal averaging of such compositional data.

The shift in equilibrium temperature accompanies a corresponding trend in fO_2 and notably oxygen fugacity relative to established and empirical mineral buffers (Fig. 3). Between 1000˚C and 1100˚C, the correspondence between our measurements and previously reported estimates (squares in Fig. 3) is close, especially considering the distinct means by which the datasets were obtained (the "Type I" gas properties were calculated from analyses made at Halema'uma'u in 1917; ref. 9). However, at temperatures below the solidus, our measurements increasingly trend towards the NNO buffer, in contrast to calculations for "Type II" gas samples collected at Kīlauea's East Rift Zone in 1983 (ref. 9). We interpret this decoupling as a further consequence of changes in bubble size, with larger bubbles increasingly unable to sustain gas-melt equilibrium as they rise (i.e., gas in bubble interiors cannot effectively exchange oxygen with the melt). However, the internal equilibrium of the gas mixture can be expected to adjust rapidly to decompression and cooling – redox kinetics involving the species of interest at magmatic temperatures are fast (timescales of order 10^{-2} s) with respect to bubble ascent rates in the conduit and lava lake[28].

To test whether closed-system cooling can explain our observations, we compute the molecular speciation and fO_2 for a gas-only mixture, as a function of temperature, starting with the observed elemental composition (C-O-S-H-Cl-F) at 1150˚C. This mimics the trend of our spectroscopic observations closely (dashed line with arrow in Fig. 3) providing compelling evidence that the internal redox state of the gas is controlled by closed-system cooling during bubble expansion, with a dominant role played by sulphur owing to its abundance and range of oxidation states. The gas-only cooling trend is extrapolated in Fig. 3 to 1200˚C, reaching the QFM redox buffer, and into the range of fO_2 reported for matrix glasses of samples from the Overlook Vent ejected in 2008 and 2010 (ref. 29).

The relationship of the fO_2-temperature trend to the rock buffers for "Type I" and "Type II" Kīlauea gases (Fig. 3) has been explained by continuous exchange of oxygen between the gas and lava, even to sub-solidus temperatures[9]. The discrepancy with our observations may reflect differences in gas/lava interaction immediately after the escape of gases from the lava surface. In the case of our measurements, there was no obstruction to gas-air exchange above the exposed lava lake. In contrast, the "Type II" gases were sampled via tubing inserted into a confined space accessed through a narrow 'vigorously fuming' fissure 1–2 m above active lava[9]. The fissure was 'closed to the atmosphere at most points', and air contamination of the samples, determined analytically, was very low[9]. These circumstances may permit oxygen exchange between gas and lava even after gases escape, and as they expand and cool in the enclosure above the lava surface.

In Fig. 4, we contrast the gas cooling for bubbles rising through a cooler, more viscous magma (10^5 Pa s, 1000°C), and a hotter, less viscous magma (10^{-1} Pa s, 1500°C) than Kīlauea's. For the high-viscosity case, the cooling is less pronounced owing to the lower rise speed of the bubble and the greater heating of the gas. The low viscosity case is intended to simulate the higher temperatures (>1400–1600°C) and more mafic melt compositionof the early Earth[30,31]. Here, the modelled cooling is somewhat less than the case for Kīlauea. As the magma becomes less viscous (10^2 to 10^{-1} Pa s), the bubbles rise with inertial speed and so temperature plays a stronger role owing to the T^4 dependence. Hence, at 1500°C, the radiative heating of the bubble is stronger. Nevertheless, the cooling remains significant, and we speculate that decametre-sized bubbles rising rapidly through such hot and fluid melt would cool by hundreds of degrees, accompanied by significant redox shifts. If this is realistic, then the redox difference between

magmas and their emitted gases should have been higher for the Early Earth making the link between Earth's atmosphere and magmatism not as straightforward as commonly assumed[32],[33].

References

[1] Gaillard, F., Scaillet, B., & Arndt, N. T. Atmospheric oxygenation caused by a change in volcanic degassing pressure. *Nature* **478**, 229-232 (2011).

[2] Simon, A.C. & Ripley, E. M. The role of magmatic sulfur in the formation of ore deposits. *Reviews in Mineralogy and Geochemistry* **73**, 513-578 (2011).

[3] Allard, P., Burton, M., & Muré, F. Spectroscopic evidence for a lava fountain driven by previously accumulated magmatic gas. *Nature* **433**, 407-410 (2005).

[4] Burton, M., Allard, P., Muré, F. & La Spina, A. Magmatic gas composition reveals the source depth of slug-driven Strombolian explosive activity. *Science* **317**, 227-230 (2007).

[5] Oppenheimer, C., et al. Mantle to surface degassing of alkalic magmas at Erebus volcano, Antarctica. *Earth and Planetary Science Letters* **306**, 261-271 (2011).

[6] Burgisser, A., & Scaillet, B. Redox evolution of a degassing magma rising to the surface. *Nature* **445**, 194-197 (2007).

[7] Moretti, R., & Papale, P. On the oxidation state and volatile behavior in multicomponent gas–melt equilibria. *Chemical Geology* **213**, 265-280. (2004).

[8] Jaupart, C. & Vergniolle, S. Laboratory models of Hawaiian and Strombolian eruptions, *Nature* **331**, 58-60 (1988).

[9] Gerlach, T. M. Oxygen buffering of Kilauea volcanic gases and the oxygen fugacity of Kilauea basalt. *Geochimica et Cosmochimica Acta* **57**, 795-814 (1993).

[10] Greenland, L. P. Gas analyses from the Pu'u O'o eruption in 1985, Kilauea volcano, Hawaii. *Bulletin of Volcanology* **48**, 341-348 (1986).

[11] Edmonds, M., et al. Magma storage, transport and degassing during the 2008–10 summit eruption at Kīlauea Volcano, Hawai‘i. *Geochimica et Cosmochimica Acta* **123**, 284-301 (2013).

[12] Edmonds, M., & Gerlach, T. M. Vapor segregation and loss in basaltic melts. *Geology* **35**, 751-754 (2007).

[13] Peters, N., Oppenheimer, C., Killingsworth, D. R., Frechette, J. & Kyle, P. Correlation of cycles in Lava Lake motion and degassing at Erebus Volcano, Antarctica, *Geochemistry, Geophysics, Geosy*stems **15**, 3244–3257, doi:10.1002/2014GC005399 (2014).

[14] Patrick, M. R., Orr, T., Swanson, D. A. & Lev, E. Shallow and deep controls on lava lake surface motion at Kīlauea Volcano. *Journal of Volcanology and Geothermal Research* **328**, 247-261 (2016).

[15] Gerlach, T. M. & Graeber E. J. Volatile budget of Kilauea volcano, *Nature* **313** 273-277 (1985).

[16] Naughton, J. J., Derby, J. V. & Glover, R. B. Infrared measurements on volcanic gas and fume: Kilauea eruption, 1968, *Journal of Geophysical Research* **74**, 3273–3277, doi:10.1029/JB074i012p03273 (1969).

[17] Patrick, M. R., Anderson, K. R., Poland, M. P., Orr, T. R. and Swanson, D. A. Lava lake level as a gauge of magma reservoir pressure and eruptive hazard. *Geology* **43**, 831-834 (2015).

[18] Dixon, J. E., Clague, D. A., & Stolper, E. M. Degassing history of water, sulfur, and carbon in submarine lavas from Kilauea Volcano, Hawaii. *The Journal of Geology* **99**, 371-394 (1991).

[19] Clague, D. A., Moore, J. G., Dixon, J. E., & Friesen, W. B. Petrology of submarine lavas from Kilauea's Puna Ridge, Hawaii. *Journal of Petrology* **36**, 299-349 (1995).

[20] Dixon, J. E. & Stolper, E. M. An experimental study of water and carbon dioxide solubilities in mid-ocean ridge basaltic liquids. Part II: applications to degassing. *Journal of Petrology* **36**, 1633-1646 (1995).

[21] Scaillet, B. & Pichavant, M. A model of sulphur solubility for hydrous mafic melts: application to the determination of magmatic fluid compositions of Italian volcanoes. *Annals of Geophysics* **48**, 671-698 (2005).

[22] Lesne, P., Scaillet, B., Pichavant, M., Iacono-Marziano, G. & Beny, J. M. The H_2O solubility of alkali basaltic melts: an experimental study. *Contributions to Mineralogy and Petrology* **162**, 133-151 (2011).

[23] Lesne, P., Scaillet, B., Pichavant, M. & Beny, J. M. The carbon dioxide solubility in alkali basalts: an experimental study. *Contributions to Mineralogy and Petrology* **162**, 153-168 (2011).

[24] Holloway, J. R. Igneous fluids. *Reviews in Mineralogy and Geochemistry* **17**, 211-233 (1987)

[25] Alletti, M., et al. Chlorine partitioning between a basaltic melt and H_2O–CO_2 fluids at Mount Etna. *Chemical Geology* **263**, 37-50 (2009).

[26] Moretti, R., et al. Degassing vs. eruptive styles at Mt. Etna volcano (Sicily, Italy). Part I: Volatile stocking, gas fluxing, and the shift from low-energy to highly explosive basaltic eruptions, *Chemical Geology* **482**, 1-17 (2018)**.**

[27] Wright, T. L., Peck, D. L. & Shaw, H. R. Kilauea Lava Lakes: Natural Laboratories for Study of Cooling, Crystallization, and Differentiation of Basaltic Magma, in *The Geophysics of the Pacific Ocean Basin and Its Margin* (eds G. H. Sutton, M. H. Manghnani, R. Moberly and E. U. Mcafee), American Geophysical Union, Washington, D.C. 375-390. doi: 10.1029/GM019p0375 (1976)

[28] Burgisser, A. et al. Backward tracking of gas chemistry measurements at Erebus volcano, *Geochemistry, Geophysics, Geosystems* **13**, *Q11010, doi:*10.1029/2012GC004243 (2012).

[29] Moussallam, Y. et al. The impact of degassing on the oxidation state of basaltic magmas: A case study of Kīlauea volcano. *Earth and Planetary Science Letters* **450**, 317-325 (2016).

[30] Elkins-Tanton, L. T. Linked magma ocean solidification and atmospheric growth for Earth and Mars. *Earth and Planetary Science Letters* **271**, 181-191 (2008).

[31] Dingwell, D. B., Courtial, P., Giordano, D., & Nichols, A. R. L. Viscosity of peridotite liquid. *Earth and Planetary Science Letters* **226**, 127-138 (2004).

[32] Li, Z. X. A. & Lee, C-T. A., The constancy of upper mantle fO_2 through time inferred from V/Sc ratios in basalts. *Earth and Planetary Science Letters* **228**, 483-493 (2004).

[33] Holland, H. D. Volcanic gases, black smokers, and the Great Oxidation Event. *Geochimica et Cosmochimica Acta* **66**, 3811-3826 (2002).

Acknowledgements

This work was supported by the Natural Environment Research Council (through the Centre for the Observation and Modelling of Volcanoes, Earthquakes and Tectonics and grant NE/N009312/1), and LabEx VOLTAIRE. Y.M. received additional support from the Leverhulme Trust. We thank Peter Kelly (USGS) for his review of the pre-submission manuscript, and three reviewers for their insightful comments on the submitted manuscript. We are grateful to Vitchko Tsanev for discussion on gas radiation at high temperature and pressure.

Author contributions

All authors contributed to preparation and revision of the manuscript. C.O. analyzed and modelled spectroscopic data; B.S. modelled the melt-inclusion data; A.W. and C.O. developed the bubble-cooling model; A.J.S. and T.E. led the field campaign; and Y.M. contributed wider context on melt redox evolution.

Competing financial interests

The authors declare no competing financial interests.

Figure captions

Fig 1. Instrument set up and lava lake behaviour at Halema'uma'u on 5 March 2013. (a) Fourier transform infrared spectrometer with 10-inch telescope pointed at the lava lake some 200 m distant; (b) initial regime of mild degassing (non-spattering); (c) subsequent regime of vigorous degassing (spattering). The lava lake is approximately 200 m across.

Fig 2. Observed and calculated gas properties for glass samples dredged from the Puna ridge. (a) Evolution of the mole fraction of water in the gas (xH_2O) with pressure; dashed-line logarithmic fit in is intended simply to guide the eye. (b) Comparison between modelled pressure of volatile saturation and the seabed pressure where each sample was collected (dashed line shows 1:1 correspondence). (c) Evolution of the SO_2/HCl molar ratio with pressure, calculated for fO_2 = NNO–0.5. Our spectroscopic measurements of gas emissions from the lava lake are indicated by square symbols in (a) and (c). Gas compositions were computed by combining thermodynamic models of H_2O and CO_2 solubilities with measured volatile contents, assuming saturation at all levels, and incorporating a model for fS_2 (ref. 21). These give the mole fractions of C-O-H-S species (i.e., H_2O, SO_2, CO_2, etc.). Temperatures for each sample were computed using a suitable geothermometer[34]. Error bars reflect ±10 ppm uncertainty in measured CO_2 contents in glass, the largest source of uncertainty (particularly at low pressure).

Fig 3. Computed equilibrium temperature and fO_2 for spectrosccopic measurements of gas emissions from Kīlauea's lava lake. The dataset is classified into mild-degassing (12:14 to 13:14 h local time) and vigorous-degassing (15:16 to 15:23 h) regimes on 5 March 2013. Also shown are NNO and QFM buffers; the solidus temperature of Kīlauea basalt; ranges of CO_2/CO

and SO_2/H_2S, temperature-fO_2 calculations for "Type I" and "Type II" gases (Kīlauea Summit and East Rift Zone emissions, respectively) and associated empirical fit[9]; and reported fO_2 at 1200˚C for 2008 and 2010 matrix glasses for ejecta from the Overlook Vent (mean and range shown)[29]. Note that, below the solidus, our analyses for 'vigorous degassing' are more oxidized than "Type II" gases at equivalent equilibrium temperatures. The white/black dashed line with arrow shows temperature-fO_2 calculations for closed-system, gas-only cooling starting with our measured gas composition at 1150˚C (open triangle), showing a close fit to the dataset.

Fig 4. Amount of gas cooling as a function of final bubble radius (at the surface) and magma viscosity. Three temperature and viscosity scenarios are shown. The 1200˚C, 10^2 Pa s case corresponds to Kīlauea lava lake; the 1000˚C, 10^5 Pa s case is applicable, for instance, to the phonolite lava lake of Erebus volcano, Antarctica; while the 1500˚C, 10^{-1} Pa s case is intended to reflect early Earth magmas.

Methods

Fourier transform infrared spectroscopy

We used a MIDAC FTIR spectrometer with a Stirling-engine-cooled MCT detector. Incoming light was collimated with a 10-inch Newtonian telescope (field of view 3 mrad). All spectra were recorded with a nominal optical path difference (retardation) of 2.0 cm, corresponding to a 0.5 cm^{-1} spectral resolution. Interferograms were Fourier transformed with a Mertz phase correction and triangular apodization. We then determined the column amounts of gases contributing to the recorded absorption spectra, employing a forward model[35] that simulates the atmospheric transmittance in several discrete wavebands using line parameters for selected gas species taken from the HITRAN database (hitran.org). The model considers a one-layer atmosphere with

pressure, temperature and initial column amounts specified for both atmospheric and volcanic gas species. Simulated spectra are adjusted to fit each observed spectrum using an optimal estimation method[36].

There are several sources of uncertainty in the retrieved column amounts, notably the limitation of assuming a single-layer atmosphere (with uniform temperature), and the sensitivity of the instrument line shape to off-axis rays striking the interferometer. Much care, therefore, needs to be exercised in defining the limits of the spectral windows used for fitting. Our retrieval procedure includes calculation of a solution covariance matrix, whose diagonal elements represent the variance of each retrieved parameter, and which provides a measure of the retrieval error for each parameter fitted in each spectrum. The measurement error required to derive the covariance matrix is given by the standard deviation of the residual in the fit (i.e., forward model minus observed spectrum). These calculated variances include contributions from the forward model error (arising from the selected instrument line shape used to represent the spectrometer's field of view and retardation), measurement noise, the information content of the measurement for each parameter fitted (dependent on the spectral microwindow for the fit), and the degrees of freedom (an inverse function of the number of parameters in the fit). Laboratory experiments using very similar equipment and retrieval methods have indicated that absolute accuracies of ~5% or better can be achieved[37].

Often, when absorption spectra such as ours are collected on a volcano over a span of an hour or so, scatter plots of retrieved column amounts for two gases are presented and used to compute average molecular ratios (e.g., CO_2/CO, CO_2/SO_2, CO_2/H_2O). These regressions may hide real source variation, however[38]. If we treat each spectrum as an individual measurement, then we can examine rapid variations in gas composition. This requires careful correction for ambient air

contributions to the measured water and CO_2 abundances. Since other measured volcanic gas species, i.e., CO, OCS, SO_2, HCl and HF are present in negligible quantities in the ambient atmosphere, we can estimate background air contributions to CO_2 and H_2O from the intercepts of linear regressions of suitable scatter plots (e.g., CO_2 *vs*. SO_2; Fig. S1). Note there is a spread of observations around the linear fit shown in the figure. A much wider variation is evident when looking at the redox pair CO_2 *vs*. CO (Fig. S2).

Our gas 'samples' represent the molecules lying within the optical path between spectrometer and lake surface (the infrared source). Thus, an individual sample is likely to contain gas just released at the lava/air interface, as well as gas that has been circulating within the crater for a period. Given the continuous dispersion of the plume by convection and advection, most of gas molecules sensed under the conditions encountered were emitted within seconds or a few tens of seconds of the measurement. Thus, each spectrum approximates the near-instantaneous emission from the lava surface. Previous studies of the lava lake at Erebus volcano, Antarctica, using similar equipment and methods have demonstrated the potential to track rapid variations in plume chemistry[13].

Calculation of redox state and temperature

Volcanic gas compositions are often evaluated in terms of redox equilibria. This permits assessment of gas-rock or gas-melt exchange, and reactions between magmatic and hydrothermal fluids, or between gases and air. We consider two here, since they represent, sample-by-sample, the relationship between temperature, pressure and fO_2 at equilibrium. We also have measurements for all the species concerned (CO, CO_2, OCS, SO_2).

The first is:

$3CO + SO_2 = 2CO_2 + OCS$ (1)

and the second:

$CO + ½O_2 = CO_2$ (2).

Equation (1) is useful because the equilibrium is a function of pressure, *p*, as well as temperature, *T* (K):

$$\log_{10}p = \frac{-15224}{T} + 9.22608 - \log_{10}\left\{\left(x_{CO}/x_{CO_2}\right)^2 . \left(x_{CO}/x_{OCS}\right) . x_{SO_2}\right\} \quad (3)$$

in which the constants (*K*), which are based on the reference state of the pure gaseous components at 1 bar, have been calculated using data tables in ref. [39] and by regressing log *K* against 1/*T* for the temperature range 727–1227°C. For each spectrum (sample), we readily obtain x_{CO}/x_{CO_2} and x_{CO}/x_{OCS} from the corrected retrieved column amounts of each gas. x_{SO_2} is obtained by normalizing all the seven species measurements (CO, CO_2, OCS, H_2O, SO_2, HCl and HF, after air correction). Adjustments can be made for estimated H_2 and H_2S abundances but these only shift computed temperatures by 1–2°C. The key assumption we then make is that the internal redox of the magmatic gas mixture equilibrates to atmospheric pressure, which is reasonable since gases will very rapidly reach equilibrium at temperatures above 800°C (ref. [40]). This enables calculation of the equilibrium gas temperature, *T* (in Kelvin), for each sample. For equation (2), the equilibrium constant, K_2, is a function of *T* and fO_2, as follows:

$CO_2/CO = K_2\sqrt{fO_2}$ (4).

This yields:

$$\log_{10}\left(\frac{x_{CO_2}}{x_{CO}}\right) = \frac{14724.5}{T} - 4.5057 + {}^{1}/_{2}\log_{10}(fO_2) \qquad (5)$$

where fO_2 is in bars and constants are again calculated from (39). Taking equilibrium T computed as above (3), we can then compute fO_2 for each sample.

For these calculations, the largest single source of uncertainty arises from the estimation of the background CO_2 and H_2O abundances (column amounts), as shown in Fig. S1. The relative error in this correction is greatest for spectra with low volcanic gas contributions, so we excluded from further analysis those spectra for which the recorded CO_2 column amount was less than 20% above background. We also looked closely at uncertainties in OCS determinations. Although the proportion of OCS that we calculate in the gas phase is only around 0.0004 mol%, the comparatively small abundance is compensated for by the strength of the molecule's absorption cross section in the mid infrared region of the spectrum, and the retrievals are robust. We excluded analyses for which the retrieved error on OCS exceeded 25%. To test the sensitivity to uncertainties in these parameters, we varied them systematically to obtain error estimates of approximately ±20°C in temperature and ±0.3 log units in fO_2, as indicated in Fig. 2. We note that the precision on the measurements is much higher because most of the error sources are systematic, and we have analysed datasets collected over short intervals of time, which minimises the effect of temporal variation in background atmospheric abundance of H_2O.

To justify further our assumption that equilibration proceeds to atmospheric pressure, we investigated the alternative scenarios. If we assume that fO_2 follows the empirical buffer reported by ref. 9, then we calculate again a wide range of equilibrium temperatures but pressures are found to be considerably less than atmospheric for most of the vigorous degassing spectra. Further, computed pressure decreases with decreasing equilibrium temperature, which we cannot

rationalize. Alternatively, if we fix the gas temperature to that of the magma, and compute fO_2 and pressure, the latter values range between 30 and 400 bars. In this case, we cannot reconcile how the emitted high-temperature gas could preserve all the way to the surface such a high-pressure signature acquired at depth.

Model for bubble cooling

To estimate cooling of a bubble of mass m rising through magma, we require a model of the rate of heat transfer, H, to the bubble from the melt, which buffers the cooling as the bubble expands. If the bubble volume changes by an amount ΔV in time Δt, the work done by the bubble is $p\Delta V$, where p is the pressure, and this, along with the heat transfer, $H\Delta t$, leads to a change in the internal energy of the bubble, $mc_g\Delta T_g$, according to the relation:

$$mc_g\Delta T_g = -p\,\Delta V + H\Delta t \qquad (6)$$

where m is the bubble mass, c_g is the specific heat capacity of the gas, and ΔT_g its change in temperature. The pressure in the conduit is approximated by the magmastatic pressure, which applies provided that the bubble concentration in the conduit remains small. For a bubble of fixed mass rising at speed u, we can express equation (6) in terms of the height of the bubble in the conduit, in differential form:

$$mc_g dT_g/dz = -p\, dV/dz + H/u \quad (7)$$

where z is the distance above a reference level. Experimental data suggest that, if the Reynolds number (Re, given by $\rho_m ur/\mu_m$ where ρ_m and μ_m are the melt density and dynamic viscosity,

respectively, and r is the bubble radius), exceeds 100, the speed follows the approximate inertial law[41]:

$$u = 0.3\sqrt{(2g\,r)} \qquad (8)$$

where g is the acceleration due to gravity. Alternatively, for $Re \lesssim 10$, the speed may be approximated by[41]:

$$u = 2g(\rho_m - \rho_g)r^2 / 9\mu_m \qquad (9)$$

where ρ_g is the gas density. We assume a simple transition from one regime to the other, as the bubble rises and Re increases, when the two speeds (8) and (9) are equal.

The heat flux, H, from the melt to the bubble depends on the bubble rise speed, and is given in terms of the average thickness of the thermal boundary layer in the melt around the bubble. As melt is displaced by the bubble, the boundary layer thickens from the top to the base of the bubble. Since the flow around the bubble has time scale $2r/u$, the average boundary layer thickness is of order $\sqrt{(\kappa_m r/u)}$, where κ_m is the thermal diffusivity of the melt. Experiments and numerical calculations[42] for spherical bubbles with low Re (<100), as is the case for the majority of calculations herein, suggest the constants of proportionality for the average heat flux from the melt, leading to the following approximate law:

$$H = (8/\pi^{1/2})\,\rho_m c_m\,\pi\,r^2\,\kappa_m\,(T_m - T_s) / (\kappa_m r/u)^{1/2} \qquad (10)$$

where c_m is the specific heat capacity of the melt, T_m its temperature, and T_s is the average surface temperature of the bubble. This heat flux balances that from the melt surface to the gas in the bubble. This involves both convective and radiative heat transfer from the bubble surface to

the gas in the bubble. The convective heat transfer, H_{conv}, scales with the Rayleigh number of the bubble, with a shape factor associated with the convective flow in the bubble. As a simplified parameterisation, we write the convective flux using the relation for high Rayleigh number convection[43]:

$$H_{conv} = 0.4\, \pi r\, \rho_g c_g \kappa_g\, [g\, (T_s - T_g)\, r^3 / T_0\, \kappa_g\, \nu_g]^{1/3}\, (T_s - T_g) \qquad (11)$$

where T_0 is a reference temperature for the gas in the bubble, here assumed to equal T_m, and κ_g and ν_g are the thermal diffusivity and kinematic viscosity of the gas, respectively. The radiative heat transfer between the melt at the surface and the gas in the bubble, H_{rad}, is given by the Stefan-Boltmann law:

$$H_{rad} = 4\pi\, r^2\, \sigma\, E(T_g, r, p)\, (T_s^4 - T_g^4) \qquad (12)$$

where σ is the Boltzmann constant and $E(T_g, r, p)$ is the emissivity of the gas in the bubble. The emissivity depends on the mean path length of the radiation passing through the bubble ($4r/3$ for a spherical geometry), with certain wavelengths of the radiation being absorbed and re-emitted by the gas. It also depends on the pressure and temperature of the gas. We simplify the estimation of emissivity by assuming that the gas is pure water vapour, which is reasonable given the high measured water contents in the pressure range of relevance (Fig. 2a). Emissivities of water at elevated temperatures and pressures have been investigated in the context of industrial furnaces and we have built an empirical model for emissivity as a function of bubble radius, gas temperature and pressure using the look up tables in ref. 44.

By equating the heat flux from (10) with the sum of heat fluxes from (11) and (12), we can find the average surface temperature of the gas bubble, T_s, in terms of the far-field magma

temperature, T_m, and the mean gas temperature within the bubble, T_g. With this value for T_s, we can calculate the heat flux using (10) and the gas temperature, T_g, of the bubble as it ascends by integration of equation (7).

We have solved the model for the case of water vapour bubbles rising from a depth of 1500 m (the depth of the magma chamber located beneath the lava lake) to the surface. We find that, as the pressure falls off towards atmospheric pressure and the bubble accelerates upwards in the uppermost conduit and lava lake, the heat flux from the magma is unable to keep pace with the work done in expanding the bubble. It is here that the cooling is most pronounced. On reaching the surface, the gas temperature may be tens or even a few hundred degrees cooler than the magma, depending on the size of the bubble and the viscosity of the magma, which control the rise speed (Fig. 4).

The temperature of the bubble surface as well as of the vapour in the bubble for a given temperature and magma viscosity is shown in Fig. S3. It is seen in this case that the surface temperature lags the gas cooling by between 5 and 50˚C.

We stress that our treatment here is simplified. There is uncertainty in the exact coefficients in (9–10), owing to the complexity of actual bubble shapes. For simplicity, we have taken them to be spherical but in reality they would have different shape factors as they stretch and become more elliptical. Also, the details of the flow associated with the convective mixing inside the bubble (9) and the model of the absorption of radiation (10) provide representative but simplified expressions for the magnitude of the heat transfer. For example, we neglect temperature variations around the bubble surface. To illustrate the sensitivity of the calculations to the detailed parameterisation, Fig. S4 compares the computed gas cooling as a function of final

bubble size for gas emissivities 0.5 and 1.5 times the values taken from the look up tables of ref. 44. While this changes the predictions, the magnitude of the cooling remains of a similar order. These changes in the value of the emissivity can be interpreted as uncertainty in the shape factor of the gas bubble, which may evolve into a non-spherical shape, as well as some of the uncertainty in the emissivity (which is only partially constrained at elevated temperatures and pressures). We conclude that these simple cooling estimates corroborate our explanation for the span of equilibrium temperatures calculated for the gas emissions from Kīlauea and evident in Fig. 3.

Some estimates of bubble sizes are quoted in the literature cited in the main text. Fig. S5 offers an impression of the sizes attained by rupturing bubbles during spatter episodes at Kīlauea.

Additional Information

Correspondence and requests for materials should be addressed to C.O. co200@cam.ac.uk

Data availability

The datasets generated and analysed during the current study are available from the corresponding author upon reasonable request and with permission of USGS Hawaiian Volcano Observatory.

References

[34] Wallace, P. & Carmichael, I.S. Sulfur in basaltic magmas. *Geochimica et Cosmochimica Acta* **56**, 1863-1874 (1992).

[35] Oppenheimer, C. & Kyle, P.R. Probing the magma plumbing of Erebus volcano, Antarctica, by open-path FTIR spectroscopy of gas emissions. *Journal of Volcanology and Geothermal Research* **177**, 743-754 (2008).

[36] Rodgers, C. D. Characterization and error analysis of profiles retrieved from remote sounding measurements, *Journal of Geophysical Research* **95***(*D5*),* 5587–5595*, doi:*10.1029/JD095iD05p05587 *(1990).*

[37] Horrocks, L. A. et al. Open-path Fourier transform infrared spectroscopy of SO_2: An empirical error budget analysis, with implications for volcano monitoring. *Journal of Geophysical Research* **106**(D21) 27,647-27,659, *doi*:10.1029/2001JD000343 (2001).

[38] Oppenheimer, C., Lomakina, A. S., Kyle, P. R., Kingsbury, N. G. & Boichu, M. Pulsatory magma supply to a phonolite lava lake. *Earth and Planetary Science Letters* **284**, 392-398 (2009).

[39] Chase, M. W. NIST-JANAF thermochemical tables, *Journal of Physical and Chemical Reference Data*, Monograph 9, American Chemical Society/American Institute of Physics/National Institute of Standards and Technology, MD (1998).

[40] Martin, R. S., Mather, T. A. & Pyle, D. M. High-temperature mixtures of magmatic and atmospheric gases, *Geochemistry, Geophysics, Geosystems* **7**, Q04006, *doi*:10.1029/2005GC001186 (2006).

[41] Clift, R., Grace, J. R. & Weber, M. E. Stability of bubbles in fluidized beds. *Industrial & Engineering Chemistry Fundamentals* **13**, 45-51 (1974).

[42] Figueroa-Espinoza, B. & Legendre, D. Mass or heat transfer from spheroidal gas bubbles rising through a stationary liquid. *Chemical Engineering Science* **65**, 6296-6309 (2010).

[43] Turner, J. S. *Buoyancy effects in fluids*. Cambridge University Press, Cambridge (1979).

[44] Alberti, M., Weber, R. & Mancini, M. Re-creating Hottel's emissivity charts for water vapor and extending them to 40 bar pressure using HITEMP-2010 data base. *Combustion and Flame* **169**, 141-153 (2016).


(a)
MIDAC
(b)
(c)

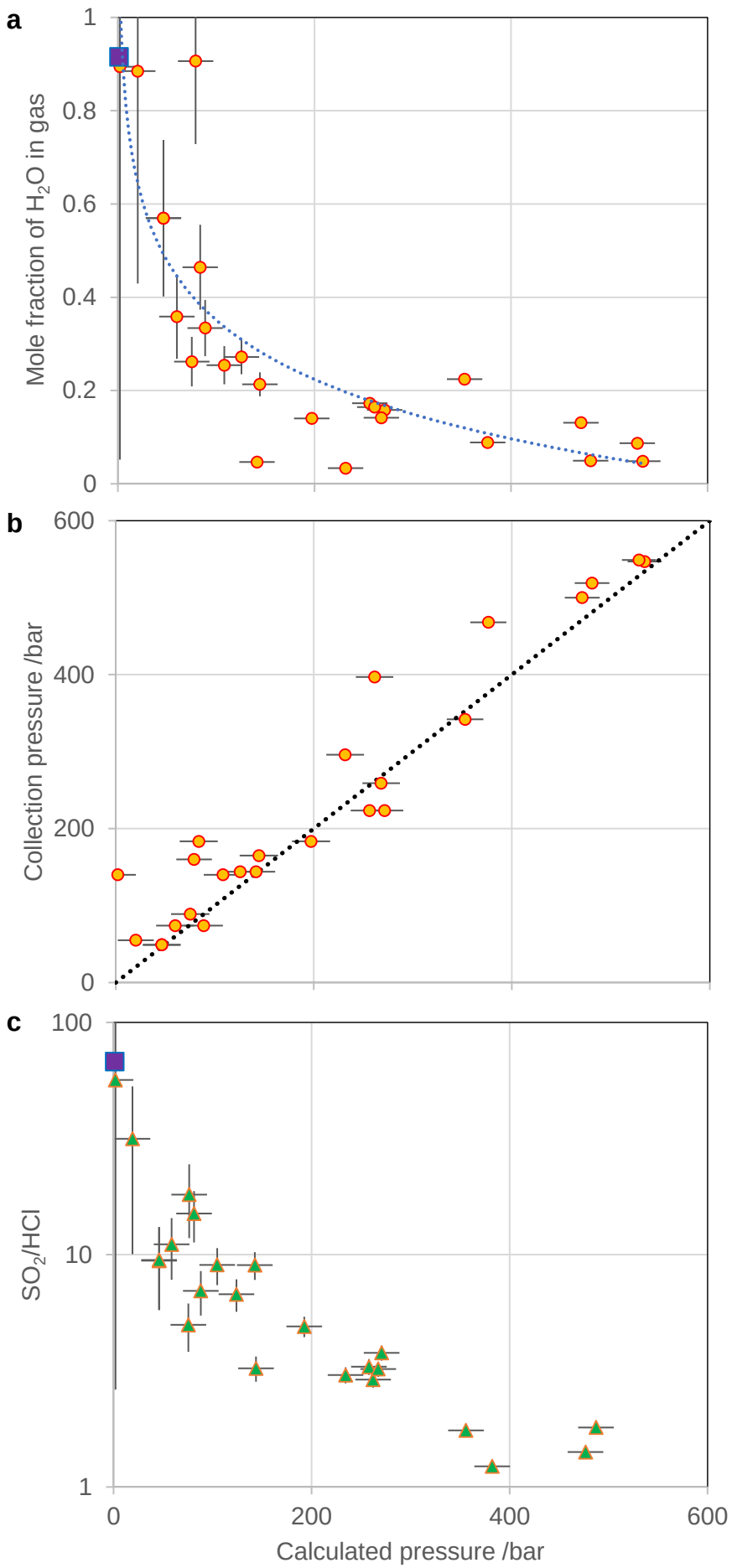
a
1
0.8
0.6
0.4
0.2
0
Mole fraction of H_2O in gas
b
600
400
200
0
Collection pressure /bar
c
100
10
1
SO_2/HCl
0
200
400
600
Calculated pressure /bar

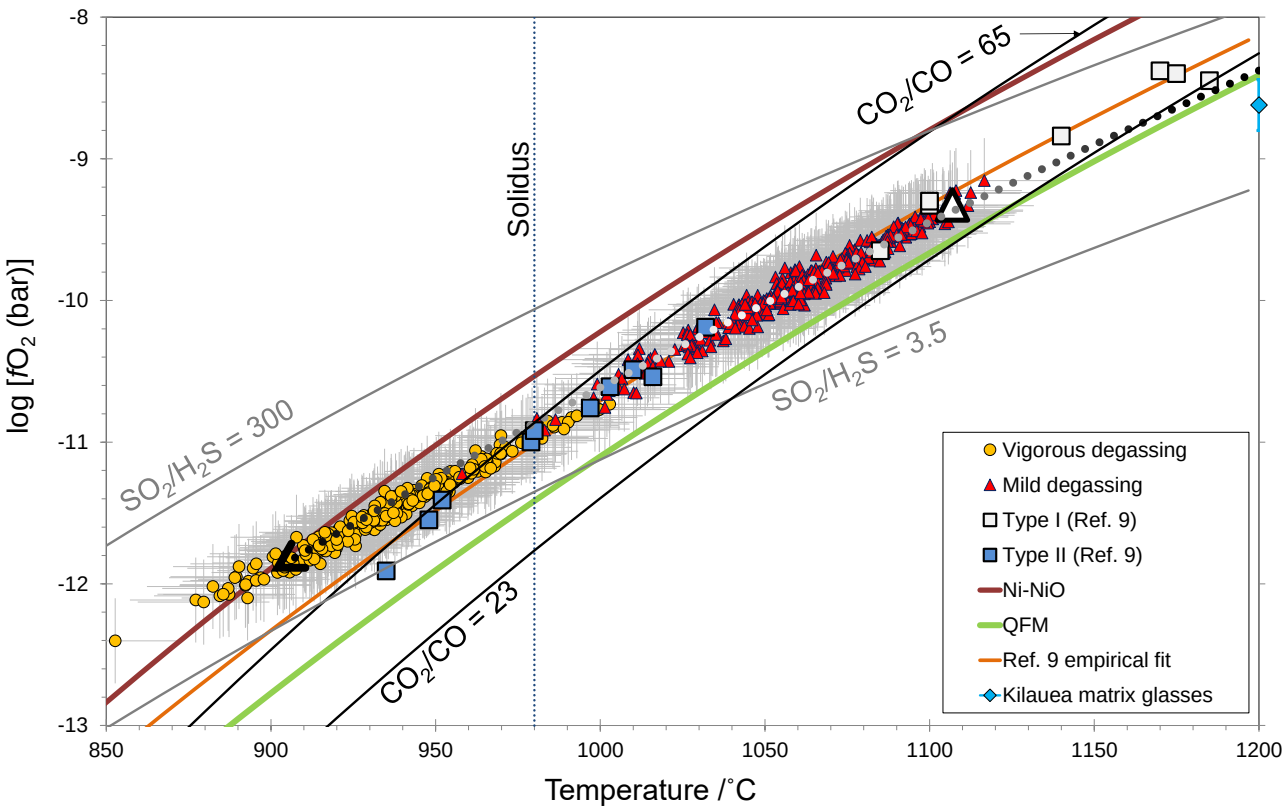
-8
-9
-10
-11
-12
-13
log [fO2 (bar)]
850
900
950
1000
1050
1100
1150
1200
Temperature /˚C
Solidus
CO2/CO = 65
CO2/CO = 23
SO2/H2S = 300
SO2/H2S = 3.5
Vigorous degassing
Mild degassing
Type I (Ref. 9)
Type II (Ref. 9)
Ni-NiO
QFM
Ref. 9 empirical fit
Kilauea matrix glasses

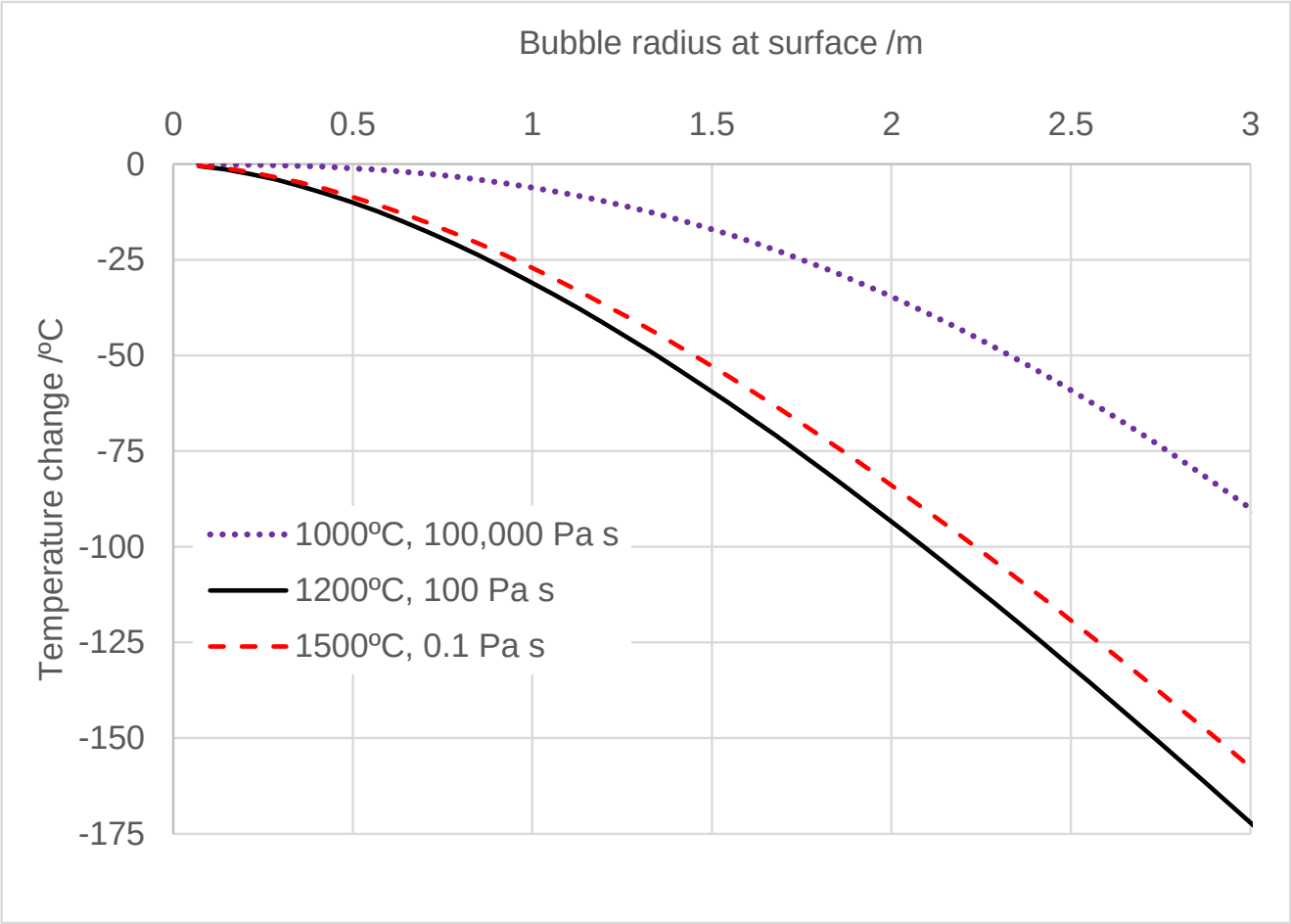
Bubble radius at surface /m
0
0.5
1
1.5
2
2.5
3
0
-25
-50
-75
-100
-125
-150
-175
Temperature change /ºC
1000ºC, 100,000 Pa s
1200ºC, 100 Pa s
1500ºC, 0.1 Pa s